Inorganic Chemistry

Article

pubs.acs.org/IC

Synthesis of Cu_2SnSe_3 Nanocrystals for Solution Processable Photovoltaic Cells

Mahshid Ahmadi,[†] Stevin S. Pramana,[‡] Sudip K. Batabyal,[§] Chris Boothroyd,[∥] Subodh G. Mhaisalkar,[†,§] and Yeng Ming Lam*[,†,§,⊥]

[†]School of Materials Science and Engineering, Nanyang Technological University, 50 Nanyang Avenue, 639798, Singapore

[‡]Facility for Analysis, Characterization, Testing and Simulation, Nanyang Technological University, 50 Nanyang Avenue, 639798, Singapore

[§]Energy Research Institute @ NTU, Nanyang Technological University, 50 Nanyang Drive, 637553, Singapore

[∥]Ernst Ruska-Centrum und Peter Grünberg Institut, Forschungszentrum Jülich, D-52425 Jülich, Germany

[⊥]Institute of Materials for Electronic Engineering II, RWTH-Aachen, Sommerfeldstr. 24, D-52074 Aachen, Germany

Supporting Information

ABSTRACT: This paper describes the synthesis of ternary chalcogenide Cu_2SnSe_3 nanocrystals as an alternative solar absorber material to conventional quaternary $CuIn_xGa_{1-x}Se_2$. We used the hot coordination solvent method with hexadecylamine as the capping ligand for the first time for this material system. Using a variety of characterization techniques, such as X-ray diffraction, selected area electron diffraction, convergent beam electron diffraction, and Raman spectroscopy, the nanocrystals were found to be monoclinic Cu_2SnSe_3 with an optical energy band gap of 1.3 eV and have a narrow size distribution. These nanocrystals are shown to be photosensitive in the range of wavelengths corresponding to the solar spectrum, which makes them highly promising as alternative photon absorber materials for photovoltaic applications.

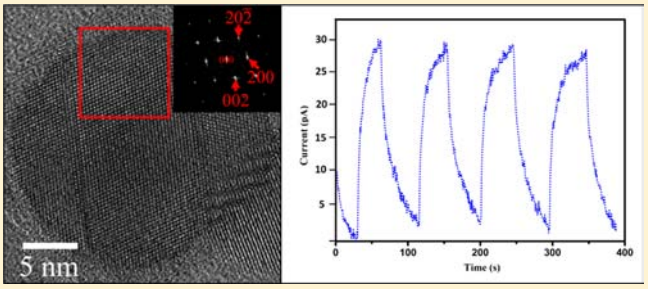

INTRODUCTION

Multicomponent chalcogenide semiconductors, such as $CuIn_xGa_{1-x}Se_2$ (CIGS), are promising candidates for solar energy harvesting, and to-date, the highest efficiency achieved for this type of solar cell is 20.3%.[1] However, due to the limited supply and increasing price of indium and gallium, there is a strong drive to find alternative materials with high abundance and low cost. Recently, there is a growing interest in two such chalcogenide semiconductor compounds, Cu_2ZnSnS_4 (CZTS) and $Cu_2ZnSnSe_4$ (CZTSe). The highest efficiency achieved for these types of solar cell is 11.1%.[2−8] When In is replaced by Sn and Ga by Zn in quaternary CZTSe, the reduction in the cost of the active material can be substantial for large-scale production. This group of semiconductors has similar electrical and optical properties to CIGS,[9−11] although, at present, the efficiency is still lower, so solar cells made using these materials still required some optimization.

In general, the more components there are in a material system, the more difficult is the composition and phase control. Complex quaternary CIGS compounds required precise control of the growth conditions, and the same goes for CZTS and CZTSe compounds. Hence, simpler ternary compound systems, such as Cu_2SnS_3 and Cu_2SnSe_3, are highly attractive, and nanocrystals of these materials are highly applicable for the fabrication of low-cost thin-film solar cells because of their solution processability. Bulk Cu_2SnSe_3 is a p-type semiconductor with a direct band gap of 0.8−1.1 eV and a high absorption coefficient (>10^4 cm^{-1}).[12−16] Cu_2SnSe_3 can have the following crystal structures: $F\bar{4}3m$ cubic (a = 5.696 Å),[17] $I\bar{4}2d$ tetragonal (a = 5.689 Å, c = 11.37 Å),[18] $C1c1$ monoclinic (a = 6.9670(3) Å, b = 12.0493(7) Å, c = 6.9453(3) Å, β = 109.19(1)°),[19] or $C1c1$ monoclinic superstructure (a = 6.9612(14) Å, b = 12.043(2) Å, c = 26.481(5) Å, β = 94.97(3)°).[20] For cubic Cu_2SnSe_3, Cu and Sn share the same atomic positions with an occupancy of 0.67 and 0.33, respectively, whereas in tetragonal Cu_2SnSe_3, Cu and Sn only share the 4b Wyckoff site (0, 0, 0.5) with an occupancy of 0.33 and 0.67, respectively, and with full occupancy of Cu at the 4a site (0, 0, 0). However, for the monoclinic structure, both Cu and Sn are ordered over the cation positions and do not share the same atomic positions. There is also a slight distortion in both the $CuSe_4$ and the $SnSe_4$ tetrahedra as compared to the cubic structure (Figure 1). Interestingly, this material was also reported to be a good candidate in various optoelectronic applications, such as highly efficient acoustic-optic and thermoelectric devices,[12,21] and a precursor material for the

Received: May 30, 2012
Published: January 28, 2013

   dx.doi.org/10.1021/ic301141w | Inorg. Chem. 2013, 52, 1722−1728

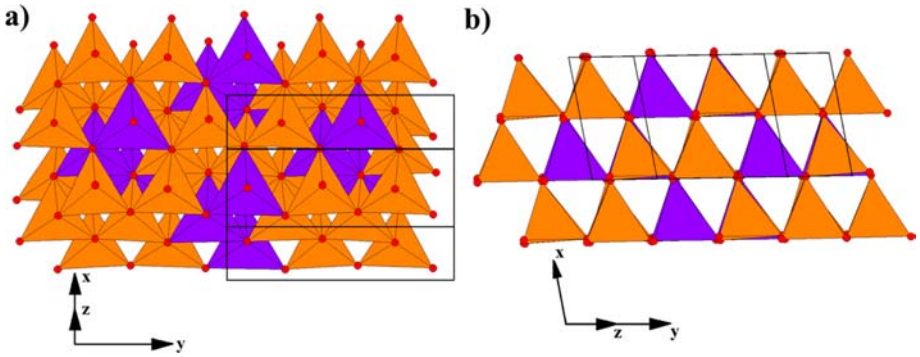

Figure 1. Representation of the crystal structure of $C1c1$ Cu_2SnSe_3 projected (a) along and (b) perpendicular to the closed packed direction, where $CuSe_4$ and $SnSe_4$ tetrahedra are drawn in orange and purple, respectively.

growth of the promising solar cell absorber, CZTSe, via a reaction of Cu_2SnSe_3 and ZnSe.[22]

The syntheses of bulk and thin films of Cu_2SnSe_3 have been reported,[12−15,23] and some of this work focuses on the synthesis of nanocrystals, for example, the colloidal synthesis of cubic nanocrystals of Cu_2SnSe_3 using oleylamine (OLA) as the coordinating solvent.[24] Most recently, nanocrystals of the wurtzite phase of Cu_2SnSe_3 were prepared using dodecylamine and 1-odecanethiol as the coordinating solvents and di-*tert*-butyl diselenide (tBu_2Se_2) as the selenium source.[25] These recent developments on the colloidal synthesis of high-quality nanostructure materials have opened up new routes for the fabrication of solution processable, low-cost, and high-efficiency printable solar cells using the nanoink concept.[26] Though some work has been done on synthesis, the understanding of the relationship between the crystal structure of Cu_2SnSe_3 nanocrystals and their optoelectronic properties is lacking. Therefore, the aim of this study is to synthesize the ternary chalcogenide Cu_2SnSe_3 nanocrystals by the hot coordination method and evaluate the potential of this compound as the photon absorber in photovoltaic cells by understanding its structural, optical, and electrical properties.

EXPERIMENTAL DETAILS

Materials. Copper(I) chloride (>99.995%), copper(II) acetate (97%), tin(IV) chloride (98%), tin(II) acetate (99%), and hexadecylamine (HDA) (98%) were purchased from Sigma-Aldrich, and selenium (Se) powder (<325 mesh, 99.7%) was obtained from Acros Organics. Acetonitrile (HPLC grade, 99.7%) was purchased from Fluka, while methanol, chloroform, and toluene are technical grade (95%).

Characterization Techniques. Ultraviolet−visible/near-infrared (UV−vis/NIR) absorption spectra of the as-synthesized nanocrystals dispersed in toluene were obtained at room temperature and under ambient conditions using a UV−vis/NIR PerkinElmer Lambda 900 spectrophotometer ($300 < \lambda < 2000$ nm, step size of 0.5 nm). The size, morphology, and crystal structure of the nanocrystals were characterized using transmission electron microscopy (TEM), selected area electron diffraction (SAED), and convergent beam electron diffraction (CBED). The samples for TEM (JEOL 2100F, with an accelerating voltage of 200 kV) were prepared by dropping nanocrystals dispersed in toluene onto lacey carbon-coated copper or nickel grids. The composition and elemental distribution of the as-prepared Cu_2SnSe_3 nanoparticles were determined semiquantitatively using energy-dispersive X-ray spectroscopy (EDX) in the TEM. Electron energy loss spectra (EELS) were collected with a Gatan imaging filter (GIF) in a Philips CM 300 TEM. The phase and crystallographic structure of the nanocrystals were characterized by grazing incidence X-ray diffraction (GIXRD) patterns, which were recorded using a Bruker D8 Advance X-ray diffractometer with Cu Kα radiation (λ_{ave} = 1.54 Å) operating at 40 kV and 40 mA. The scanning was conducted with a fixed θ of 0.5°, a scanning rate of 0.2° min^{-1}, a step size of 0.02°, and a 2θ range from 10° to 80°. Rietveld refinement was done using cubic, tetragonal, and monoclinic Cu_2SnSe_3 models.[17−20] The fundamental parameters peak-shape profile was used; a five-coefficient Chebychev polynomial and $1/x$ background, zero error, scale factors, unit cell parameters, and crystal size were sequentially refined using the TOPAS V4 program. Fractional coordinates, occupancies, and the atomic displacement factors were fixed to the values obtained from the database. To determine how reliable the fit is in TOPAS, several criteria are used, and they are the following: R_{wp}, R weighted pattern; R_{exp}, R expected; R_B, R Bragg; and χ^2 (goodness of fit) = $(R_{wp})/(R_{exp})$.

$$R_{exp} = \sqrt{\frac{\sum M - P}{\sum W_m Y_{o,m}^2}} \quad (1)$$

$$R_{wp} = \sqrt{\frac{\sum w_m (Y_{o,m} - Y_{c,m})^2}{\sum w_m Y_{o,m}}} \quad (2)$$

$$R_B = \frac{\sum |I_{\text{“o”},k} - I_{c,k}|}{\sum I_{\text{“o”},k}} \quad (3)$$

$$\text{GOF} = \chi^2 = \frac{R_{wp}}{R_{exp}} = \sqrt{\frac{\sum w_m (Y_{o,m} - Y_{c,m})^2}{M - P}} \quad (4)$$

$Y_{o,m}$ and $Y_{c,m}$ are the observed and calculated data, respectively, at data point m, M is the number of data points, P is the number of parameters, w_m is the weighting given to data point m, and $I_{\text{“o”},k}$ and $I_{c,k}$ are the observed and calculated intensities of the kth reflection.

Further evidence for composition and valence state of the product was acquired using the ESCALABMK II X-ray photoelectron spectroscopy (XPS), with Mg Kα X-ray as the excitation source. The binding energies obtained from the XPS analysis were corrected with C 1s to 284.60 eV. The micro-Raman spectra were recorded from 50 to 600 cm^{-1} by using an XY Dilor-JobinYvon-Spex spectrometer attached to an Olympus microscope, equipped with a double monochromator and a multichannel detection system. The 633.8 nm He−Ne laser line was used as an irradiator source with a power irradiance of 20 mW. Cyclic voltammetry (CV) measurements were performed on an Autolab PG302N electrochemical workstation. Carbon and gold electrodes were used as working and counter electrodes, respectively. The reference electrode was a Ag/AgCl electrode with 0.1 M tetrabutylammonium hexafluorophosphate ($TBAPF_6$) dissolved in acetonitrile as the supporting electrolyte. The ferrocene/ferrocenium couple was utilized as an internal standard.[27] A few drops of diluted nanocrystals in chloroform were deposited onto the surface of the working electrode to form a nanocrystal film. The scan rate was set at 100 mV/s, and during all the measurements, the electrolyte solution was deoxygenated by bubbling

dx.doi.org/10.1021/ic301141w | Inorg. Chem. 2013, 52, 1722−1728

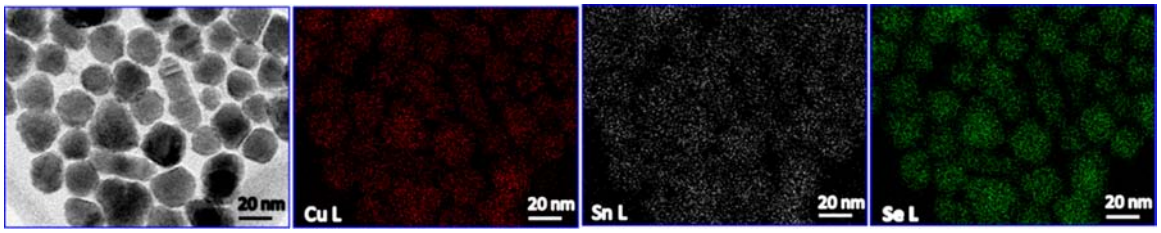

Figure 2. Bright-field TEM image of Cu_2SnSe_3 nanocrystals and corresponding EDX elemental maps.

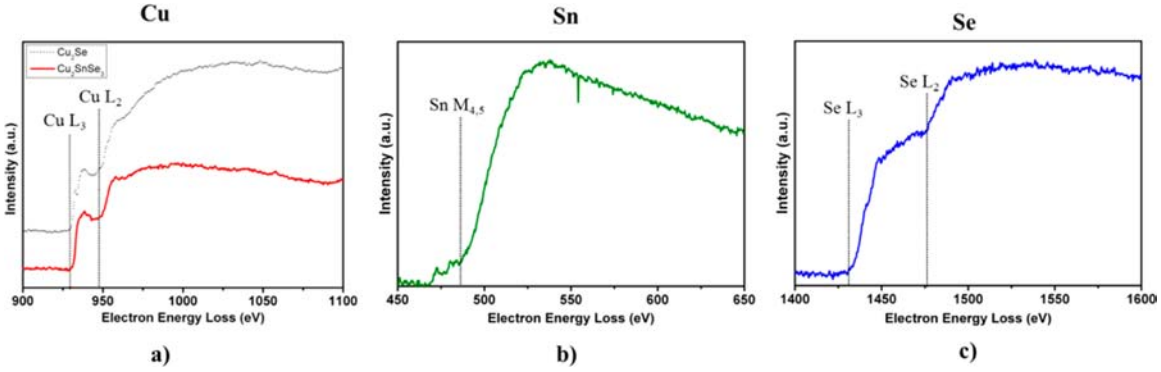

Figure 3. EELS spectra obtained from the Cu_2SnSe_3 nanocrystals and shown after background subtraction: (a) Cu L with the Cu L edge from Cu_2Se shown dotted, (b) Sn M, and (c) Se L edges. The original EELS spectra before background subtraction are shown in Figure S6 (Supporting Information).

N_2 gas through it for 10 min. The photosensitivity of the nanocrystal film was recorded using a Keithley 4200 parametric analyzer in a TTP-6 (Lakeshore Cryogenic) probe station at ambient condition. A halogen light source was used as the white-light source for the irradiation of the film.

Synthesis of Cu_2SnSe_3 Nanocrystals. Cu_2SnSe_3 nanocrystals were synthesized using the hot coordination solvent method since this method has been shown to give very good control over composition and morphology for a wide range of semiconducting chalcogenide nanocrystals.[28−31] The reaction was started by heating a stoichiometric mixture of $SnCl_4$ (0.1 mmol), CuCl (0.2 mmol), and 6.5 g of HDA in a 50 mL three-neck flask in an oxygen-free environment to 80 °C and degassing for 1 h. The complete dissolution of the cation precursors at around 140 °C was confirmed by a change of color of the solution to yellow. A mixture of 0.3 mmol of selenium powder in 4 g of HDA was heated to 50 °C in order to melt the HDA and form a suspension. This was then injected into the reaction flask at 140 °C under constant stirring and a nitrogen flow. The mixture was further heated to 240 °C and held for an hour. After the reaction was complete, the mixture was cooled down to 60 °C. Toluene and methanol were added to the solution, and the mixture was sonicated for 10 min to remove all the free ligands and also the unreacted precursors. The solution was then centrifuged at 9000 rpm for 20 min, followed by 7000 rpm for 10 min. The supernatant was discarded for each cycle in the centrifuge, and the nanocrystals were redispersed in toluene before the next cycle. The purified precipitates were subsequently redissolved in toluene or chloroform for further characterization.

RESULTS AND DISCUSSION

Both reaction parameters and precursors determine the phase and morphology of the desired product (Figures S1−S3, Supporting Information). Among the potential capping ligands reported, hexadecylamine (HDA) was chosen as it has been shown to be an effective capping ligand for the synthesis of CIGS nanocrystals, resulting in a narrow size distribution,[32] and generally, amines facilitate the formation of nanoparticles at lower temperatures.[33] The injection temperature for the hot coordination method controls the size and morphology of the nanocrystals formed (Figure S3, Supporting Information). The optimum reaction temperature was found to be 240 °C, and this temperature is similar to that previously reported for the synthesis of CIGS nanocrystals.[32] In this paper, monodisperse nanocrystals of Cu_2SnSe_3 with uniform shapes and sizes were successfully synthesized by injecting Se at 140 °C using hexadecylamine (HDA) as the capping ligand and then increasing the reaction temperature to 240 °C.

Compositional and Structural Analysis. A semiquantitative energy-dispersive X-ray spectroscopy (EDX) analysis revealed that the Cu/Sn/Se ratio was 2.1:0.9:3, close to the nominal composition (Figure S4, Supporting Information). The elements were homogeneously distributed within the nanocrystals, and there was no considerable compositional variation among the nanocrystals (see the EDS maps in Figure 2). In addition, from the X-ray photoelectron spectra (XPS) (Figure S5, Supporting Information), it is possible to deduce that the valence states of Cu, Sn, and Se are +1, +4, and −2, respectively, which confirms the formation of Cu_2SnSe_3.[34−36]

To determine the bonding state and the local electronic state of the elements in the synthesized nanocrystals, EELS spectra were collected. The Cu, Sn, and Se EELS edges are shown in Figure 3, confirming the presence of these three elements. The shape of an EELS edge is characteristic of the oxidation state and local bonding around each atom. Thus, to determine the oxidation state of Cu, we initially compared the Cu edge (Figure 3a) with edges from Cu oxides with oxidation states of Cu^0, Cu^I, and Cu^{II} but found a poor match. This is because the electronic environment of Cu bonded to O is different from that for Cu bonded to Se. When compared with the Cu edge from Cu_2Se, a better match was found (dotted line in Figure 3a), consistent with Cu in Cu_2SnSe_3 having an oxidation state of Cu^I. The Cu edge shape is also close to that reported for $Cu_2^IZnSnSe_4$[37] and Cu^IInSe_2 nanocrystals.[38]

dx.doi.org/10.1021/ic301141w | Inorg. Chem. 2013, 52, 1722−1728

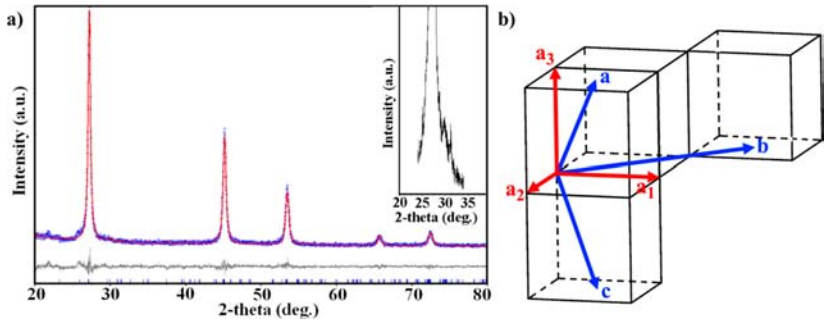

Figure 4. (a) X-ray diffraction pattern and Rietveld refinement of phase-pure monoclinic Cu_2SnSe_3 nanocrystals. The blue circles are the experimental plot, and the red line is the calculated plot of the Rietveld refinement. The gray line is the difference between the calculated and experimental intensities, and the vertical lines show the positions of Bragg peaks corresponding to monoclinic Cu_2SnSe_3. The inset shows the low-intensity reflection acquired with a longer scanning time (60 s/step) with a step size of 0.02° over the 2θ angular range from 24° to 30°. (b) The relationship between the monoclinic and pseudocubic subcells.[38].

Table 1. Refined Crystallite Size, Unit Cell Parameters, and Reliability Factors from Rietveld Refinement of the X-ray Powder Diffraction Pattern

unit cell parameters					reliability factors			crystallite size
a	b	c	V	β	R_{wp}	R_B	χ^2	
6.981 ± 0.002 Å	12.072 ± 0.004 Å	6.952 ± 0.002 Å	553.6 ± 0.3 Å^3	109.12 ± 0.02°	9.4	3.03	1.26	20 nm

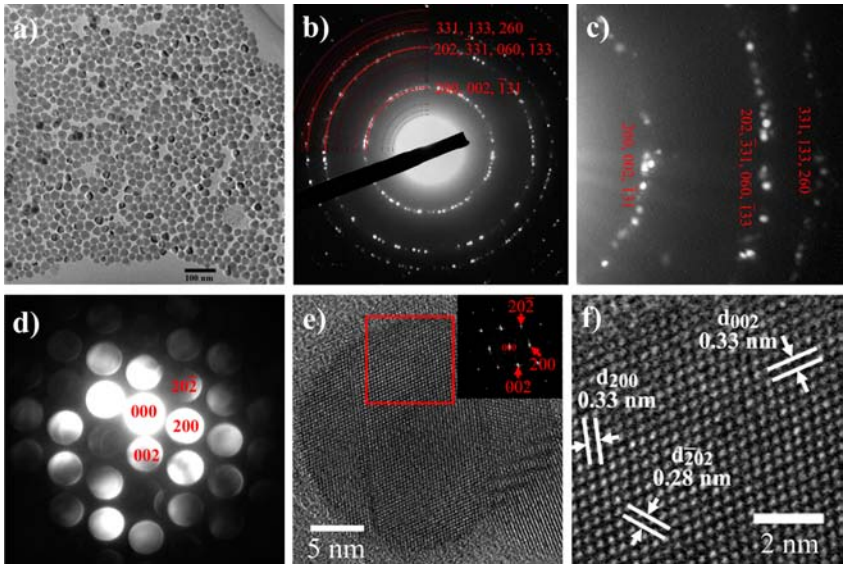

Figure 5. (a) Low-magnification TEM image of synthesized Cu_2SnSe_3 nanocrystals showing the nanocrystals' size distribution. (b) SAED pattern from an area of nanocrystals. (c) Enlarged SAED pattern showing the presence of a number of extra weak reflections next to the stronger Cu_2SnSe_3 rings. (d) CBED pattern of a single nanocrystal taken along the [010] zone axis. (e) HRTEM image of a single Cu_2SnSe_3 nanocrystal taken along [010] with inset diffractogram. (f) Enlarged HRTEM image with the plane spacings marked.

Because Cu_2SnSe_3 has been known to crystallize in different space groups,[17−20] X-ray powder diffraction studies was used to determine the structure of Cu_2SnSe_3. The starting Rietveld refinement model used the highest symmetry cubic, resulting in R_{wp} = 10.3, R_B = 4.96, and GOF = 1.32. As the major intense XRD peaks for cubic, tetragonal, and monoclinic crystal structures are common (Figure S7, Supporting Information), high-resolution analysis involving a longer scanning time (60 s/step) with a step size of 0.02° over a 2θ angular range from 24° to 30° was required to distinguish the lower symmetry structures. As a result, a minor reflection at 2θ = 29.72 (inset of Figure 4a) was seen, which is attributed to the monoclinic structure. From the Rietveld refinement of the pattern using the monoclinic model, values of R_{wp} = 9.4, R_B = 3.03, and GOF = 1.26 were obtained (Figure 4a and Table 1). The improvement in the residuals suggests that the nanocrystals have the monoclinic $C1c1$ structure. Cu_2SnSe_3 nanoparticles reported by Sharma et al. and Jeong et al. were found to have cubic and wurtzite structures.[23,24] The relationship between the monoclinic and pseudocubic subcells is given by[39]

$$\boldsymbol{a} = \boldsymbol{a_1}/2 + \boldsymbol{a_2}/2 + \boldsymbol{a_3},$$
$$\boldsymbol{b} = 3\boldsymbol{a_1}/2 - 3\boldsymbol{a_2}/2, \text{ and}$$
$$\boldsymbol{c} = \boldsymbol{a_1}/2 + \boldsymbol{a_2}/2 - \boldsymbol{a_3} \quad (5)$$

where $\boldsymbol{a}$, $\boldsymbol{b}$, and $\boldsymbol{c}$ are the monoclinic lattice vectors, and $\boldsymbol{a_1}$, $\boldsymbol{a_2}$, and $\boldsymbol{a_3}$ are pseudocubic vectors (Figure 4b). There is also a

dx.doi.org/10.1021/ic301141w | Inorg. Chem. 2013, 52, 1722−1728

monoclinic $C1c1$ Cu_2SnSe_3 phase with a larger unit cell whose presence cannot be discounted. This superstructure is a low-temperature crystal structure that has a volume 4 times larger than that of the parent monoclinic structure.[20] However, at present, it is not possible to conclusively prove the existence of this phase due to the limitations of powder XRD.

High-resolution transmission electron microscopy (HRTEM), convergent beam electron diffraction (CBED),and select area electron diffraction (SAED) of the nanocrystals provide further structural confirmation (Figure 5b–f). The strong reflections in the diffraction pattern (Figure 5d) correspond to the monoclinic structure of Cu_2SnSe_3. Interestingly, SAED showed the presence of a number of extra weak reflections in the intense reflection rings (Figure 5c). These extra spots may suggest the lower symmetry of the Cu_2SnSe_3 structure. CBED patterns and HRTEM images were taken along the [010] zone axis, and the d-spacings were found to be d_1 = 0.28 nm, d_2 = 0.33 nm, and d_3 = 0.33 nm, corresponding to the $(20\bar{2})$, (200), and (002) crystal planes, which are consistent with the XRD results obtained for monoclinic Cu_2SnSe_3 (Figure 5d–f) (see Table S1 (Supporting Information) for the refined structure factors for $C1c1$ Cu_2SnSe_3). The diameter of the nanocrystals estimated from the TEM image in Figure 5a is about 20 nm, consistent with the value calculated from the XRD pattern based on the volume-weighted column length (Table 1) with a narrow size distribution. Figure S8 (Supporting Information) shows the nanocrystal size distribution obtained by measuring 220 individual nanoparticles with the average size of 20 nm.

Raman spectroscopy, where direct information about the vibrational properties of crystalline materials can be obtained, has shown to be a useful tool for the characterization of semiconductors, where direct information about the vibrational properties of crystalline materials can be obtained. Figure 6

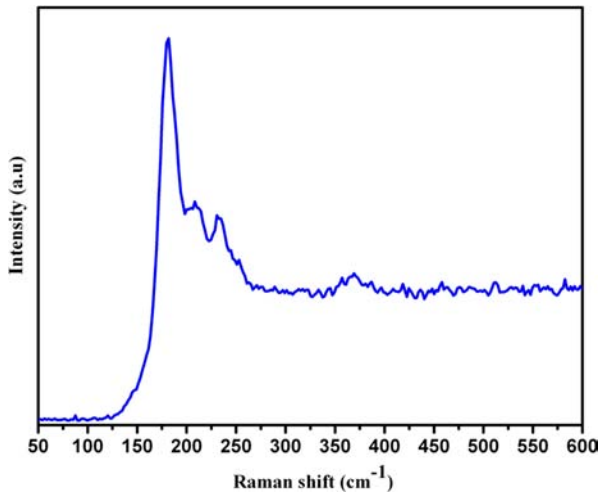

Figure 6. Raman spectrum from Cu_2SnSe_3 nanocrystals.

shows the unpolarized room-temperature Raman spectrum of the as-synthesized Cu_2SnSe_3 nanocrystals. Four peaks listed in Table S2 (Supporting Information), an intense peak at 180 cm^{-1} and a broad peak at 200 and 230 cm^{-1}, are attributed to the Cu_2SnSe_3 phase, and this is in agreement with work reported earlier.[40] The most intense peak at around 180 cm^{-1} can be attributed to the strongest Á mode and resembles the vibration of an anion atom with cations at rest. The Raman shifts for monoclinic Cu_2SnSe_3 ($C1c1$ space group and 2 Cu, 1 Sn, and 3 Se atoms in 4a Wyckoff positions) have been calculated and correspond very well to previously reported data and to our observation (see Table S2, Supporting Information), confirming that our Cu_2SnSe_3 has the monoclinic structure.[41,42] Together with the XRD data, it provides strong proof that the nanocrystals are monoclinic. We also collected Raman spectra from above 500 cm^{-1} in order to determine whether the secondary phase, $Cu_{2-x}Se$, is present. No evidence of any secondary phase, particularly the $Cu_{2-x}Se$ phase (which has a peak at around 520 cm^{-1}), was found.[43]

Optical and Electrical Analysis. The absorption properties of Cu_2SnSe_3 nanocrystals were evaluated using UV–vis spectroscopy. The absorption spectrum of the Cu_2SnSe_3 nanocrystals shown in Figure 7a exhibits a broad absorption band in the visible range with a tail extending to the infrared regime. The band gap of the synthesized Cu_2SnSe_3 nanocrystals is estimated to be around 1.3 eV, as shown in the inset of Figure 7a. The estimated band gap is consistent with that obtained from the PL spectrum of a single Cu_2SnSe_3 grain reported by Altosaar et al.[42] There is a wide range of band-gap energies reported for this compound. For bulk Cu_2SnSe_3 synthesized by the vertical Bridgman–Stockbarger technique and sputtered thin films, the band gap was found to be 0.84 eV.[12,14] Thin-film Cu_2SnSe_3 prepared by coevaporation onto a glass substrate with an average grain size of 600 nm was found to have two direct transitions at 0.74 and 1.12 eV.[13] On the other hand, the energy band gap of thin-film Cu_2SnSe_3 prepared by coevaporation onto a soda lime glass substrate and then annealed at 573 K was found to be 0.9 eV.[44] These observations show that the band gap of nanocrystals generally shifts to a higher energy from bulk and thin-film Cu_2SnSe_3, and this is most probably related to the quantum size effect. The most recently reported optical and electrochemical energy band gaps for cubic and wurtzite Cu_2SnSe_3 nanocrystals are 1.5 and 1.7 eV, respectively.[25] In general, it is not easy to elucidate the reason for the discrepancies in the energy band gap due to the wide range of different sample preparation and characterization techniques. Our observed optical band gap is in the range of reported values for nanocrystalline Cu_2SnSe_3.

Another way to determine the band gap as well as the energy levels of the valence band and conduction band of inorganic semiconductor nanocrystals is through the use of cyclic voltammetry (CV) to electrochemically measure the reduction and oxidation potentials.[45–47] The as-deposited Cu_2SnSe_3 nanocrystals were first dipped into a 0.1 M solution of hydrazine in acetonitrile for 30 s to remove the capping ligands. The valence and conduction bands of the inorganic semiconductors can be calculated based on the known HOMO/LUMO levels of ferrocene using the following equation (where E_{FC} is the oxidation onset of ferrocene):[27]

$$E_{HOMO/LUMO} = [(E_{ox/red} - E_{FC}) + 4.7]\ \text{eV} \quad (6)$$

The oxidation process is related to the injection of a hole into the HOMO level of organic molecules or valence band of inorganic semiconductors, and the reduction process is related to the injection of an electron into the LUMO level or conduction band of inorganic semiconductors. The CV scan for Cu_2SnSe_3 is shown in Figure 7b. The calculated valence and conduction bands from the CV results are −5.4 and −3.9 eV, respectively, and the electrochemical band gap of Cu_2SnSe_3 nanocrystals was found to be 1.5 eV, which is a little higher than the estimated optical band gap. Similar differences were

dx.doi.org/10.1021/ic301141w | Inorg. Chem. 2013, 52, 1722–1728

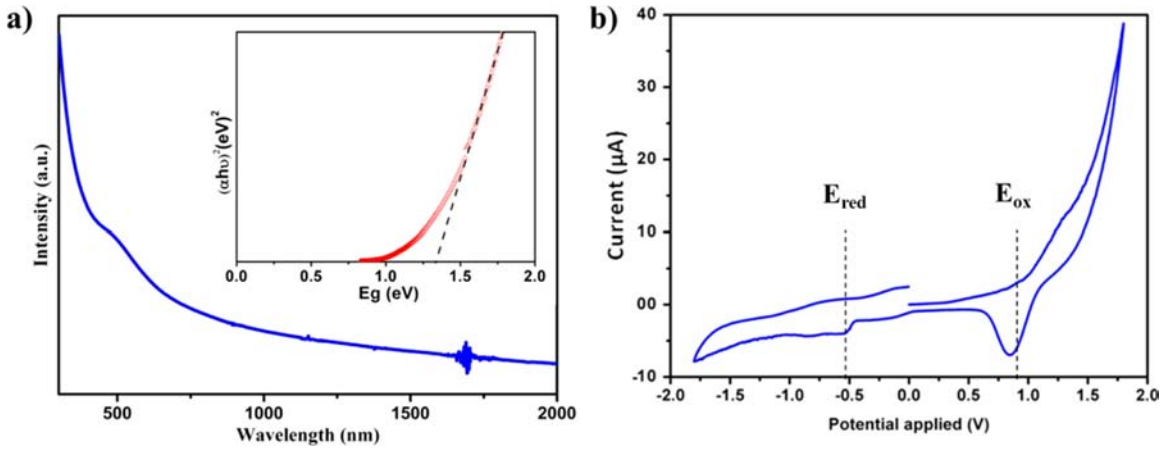

Figure 7. (a) Room-temperature UV–vis absorption spectra of monoclinic Cu_2SnSe_3 nanocrystals, and the inset shows how the band gap is determined for these nanocrystals. (b) Cyclic voltammetry measurement from monoclinic Cu_2SnSe_3 nanocrystals treated with hydrazine.

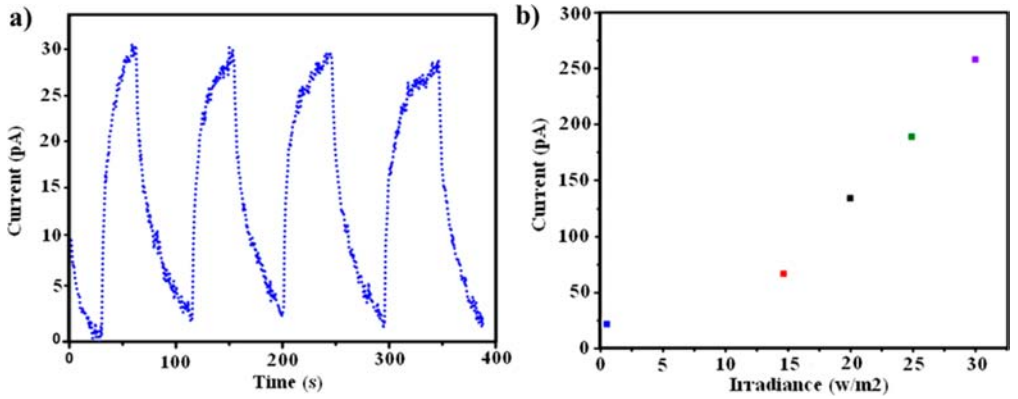

Figure 8. (a) Photoresponsiveness of the nanocrystal film at an incident light intensity of 30 W/m^2 and a bias voltage of 0.05 V. (b) Dark current and photocurrents as a function of light intensity at a bias voltage of 0.1 V.

also seen for band-gap measurement of CdSe, $CdSe_xTe_{1-x}$, and CdTe tetrapods.[46]

The energy band gap of Cu_2SnSe_3 calculated from the optical and electrochemical measurements was found to range from 1.3 to 1.5 eV, and this is essentially very close to the optimum band gap of 1.4 eV for photovoltaic devices. This suggests that this material may be a good alternative candidate for solution processable solar cells.

To evaluate the potential of this material for solar cell applications, the photoresponsiveness of these nanocrystals was also measured. Both the photocurrent stability and the photosensitivity of the as-prepared nanocrystal film were measured under alternating light and dark conditions. The incident light intensity used was 30 W/m^2, and a bias voltage of 50 mV was applied. The photoresponse from the Cu_2SnSe_3 nanocrystals is shown in Figure 8a. In the dark, the current was only 0.15 pA. However, with an incident light intensity of 30 W/m^2, the current could reach up to 30 pA, giving a photosensitivity of about 200. The photosensitivity of the nanocrystal film was further confirmed using photocurrent measurements of the sample at different incident light intensities. As shown in Figure 8b, when the intensity of the light was increased, the photocurrent of the nanocrystals increased accordingly. The photosensitivity of the Cu_2SnSe_3 nanocrystals has not been studied in detail by others, but our calculated value from the photoreponse measurement is in good agreement with the composite system of related materials.[36,48] Therefore, these results demonstrate the potential of Cu_2SnSe_3 nanocrystals as a photon absorber material in solution processable solar cells.

CONCLUSIONS

In conclusion, we have synthesized highly crystalline Cu_2SnSe_3 nanocrystals with a narrow size distribution using the hot coordination solvent method. A crystallochemical study using XRD, SAED, CBED, electron energy loss, X-ray photoelectron, and Raman spectroscopies revealed that the Cu_2SnSe_3 nanocrystals have the monoclinic $C1c1$ space group with lattice parameters a = 6.981 ± 0.002 Å, b = 12.072 ± 0.004 Å, c = 6.952 ± 0.002 Å, and β = 109.12 ± 0.02°. The nanocrystal film shows a photoresponse of 200 under illumination. The band gap of the synthesized nanocrystals was deduced from UV–vis spectroscopy and cyclic voltammetry and corresponded very well to the optimum band gap for solar energy absorption. Hence, this makes them suitable as potential candidates for the development of solution processable low-cost photovoltaic devices.

ASSOCIATED CONTENT

Supporting Information

TEM images and XRD spectra of as-synthesized nanocrystals using different precursors, TEM images of as-synthesized nanocrystals in different Se injection temperatures, EDX spectrum of Cu_2SnSe_3 nanocrystals, XPS analysis of as-

dx.doi.org/10.1021/ic301141w | Inorg. Chem. 2013, 52, 1722–1728

synthesized Cu_2SnSe_3 nanocrystals, XRD pattern of synthesized Cu_2SnSe_3 nanocrystals and the simulated XRD patterns of monoclinic and cubic Cu_2SnSe_3, representative size distribution histogram of as-synthesized Cu_2SnSe_3 nanocrystals, refined structure factors for different *hkl* of *C*1*c*1 Cu_2SnSe_3, and calculated Raman data. This material is available free of charge via the Internet at http://pubs.acs.org.

AUTHOR INFORMATION

Corresponding Author

*E-mail: ymlam@ntu.edu.sg.

Notes

The authors declare no competing financial interest.

ACKNOWLEDGMENTS

We thank the National Research Foundation and A*Star, Singapore, for providing financial and scholarship support. The electron microscopy and XRD work were performed at the Facility for Analysis, Characterization, Testing, and Simulation (FACTS) in Nanyang Technological University, Singapore.

REFERENCES

(1) Jackson, P.; Hariskos, D.; Lotter, E.; Paetel, S.; Wuerz, R.; Menner, R.; Wischmann, W.; Powalla, M. *Prog. Photovoltaics* **2011**, *19*, 894.

(2) Ahmed, S.; Reuter, K. B.; Gunawan, O.; Guo, L.; Romankiw, L. T.; Deligianni, H. *Adv. Energy Mater.* **2012**, *2*, 253.

(3) Todorov, T. K.; Reuter, K. B.; Mitzi, D. B. *Adv. Mater.* **2010**, *22*, E156.

(4) Guo, Q.; Ford, G. M.; Yang, W.-C.; Walker, B. C.; Stach, E. A.; Hillhouse, H. W.; Agrawal, R. *J. Am. Chem. Soc.* **2010**, *132*, 17384.

(5) Barkhouse, D. A. R.; Gunawan, O.; Gokmen, T.; Todorov, T. K.; Mitzi, D. B. *Prog. Photovoltaics* **2012**, *20*, 6.

(6) Todorov, T. K.; Tang, J.; Bag, S.; Gunawan, O.; Gokmen, T.; Zhu, Y.; Mitzi, D. B. *Adv. Energy Mater.* **2012**, *3*, 34−38.

(7) Jimbo, K.; Kimura, R.; Kamimura, T.; Yamada, S.; Maw, W. S.; Araki, H.; Oishi, K.; Katagiri, H. *Thin Solid Films* **2007**, *515*, 5997.

(8) Gunawan, O.; Todorov, T. K.; Mitzi, D. B. *Appl. Phys. Lett.* **2010**, *97*, 233506.

(9) Tanaka, T.; Nagatomo, T.; Kawasaki, D.; Nishio, M.; Guo, Q.; Wakahara, A.; Yoshida, A.; Ogawa, H. *J. Phys. Chem. Solids* **2005**, *66*, 1978.

(10) Riha, S. C.; Parkinson, B. A.; Prieto, A. L. *J. Am. Chem. Soc.* **2009**, *131*, 12054.

(11) Ito, K.; Nakazawa, T. *Jpn. J. Appl. Phys.* **1988**, *27*, 2094.

(12) Marcano, G.; Rincon, C.; de Chalbaud, L. M.; Bracho, D. B.; Perez, G. S. *J. Appl. Phys.* **2001**, *90*, 1847.

(13) Babu, G. S.; Kumar, Y. B. K.; Reddy, Y. B. K.; Raja, V. S. *Mater. Chem. Phys.* **2006**, *96*, 442.

(14) Kuo, D.-H.; Haung, W.-D.; Huang, Y.-S.; Wu, J.-D.; Lin, Y.-J. *Surf. Coat. Technol.* **2010**, *205*, (Suppl. 1), S196.

(15) Kuo, D.-H.; Haung, W.-D.; Huang, Y.-S.; Wu, J.-D.; Lin, Y.-J. *Thin Solid Films* **2010**, *518*, 7218.

(16) Hema Chandra, G.; Lakshmana Kumar, O.; Prasada Rao, R.; Uthanna, S. *J. Mater. Sci.* **2011**, *46*, 6952.

(17) Rivet, J. *Ann. Chim. Phys.* **1965**, *10*, 243.

(18) Hahn, H.; Klingen, W.; Ness, P.; Schulze, H. *Naturwissenschaften* **1966**, *53*, 18.

(19) Delgado, G. E.; Mora, A. J.; Marcano, G.; Rincón, C. *Mater. Res. Bull.* **2003**, *38*, 1949.

(20) Gulay, L. D.; Daszkiewicz, M.; Ostapyuk, T. A.; Klymovych, O. S.; Zmiy, O. F. *Acta Crystallogr., Sect. C* **2010**, *66*, i58.

(21) Skoug, E. J.; Cain, J. D.; Morelli, D. T. *J. Alloys Compd.* **2010**, *506*, 18.

(22) Wibowo, R. A.; Jung, W. H.; Al-Faruqi, M. H.; Amal, I.; Kim, K. H. *Mater. Chem. Phys.* **2010**, *124*, 1006.

(23) Sharma, B. B.; Ayyar, R.; Singh, H. *Phys. Status Solidi A* **1977**, *40*, 691.

(24) Jeong, J.; Chung, H.; Ju, Y. C.; Moon, J.; Roh, J.; Yoon, S.; Do, Y. R.; Kim, W. *Mater. Lett.* **2010**, *64*, 2043.

(25) Norako, M. E.; Greaney, M. J.; Brutchey, R. L. *J. Am. Chem. Soc.* **2011**, *134*, 23.

(26) Soga, T. *Nanostructured Materials for Solar Energy Conversion*, 1st ed.; Elsevier: Amsterdam, 2006.

(27) Bard, A. J.; Faulkner, L. R. *Electrochemical Methods: Fundamentals and Applications*, 2nd ed.; John Wiley: New York, 2001.

(28) Kudera, S.; Carbone, L.; Manna, L.; Parak, W. J.; Rogach, A. L. Growth Mechanism, Shape and Composition Control of Semiconductor Nanocrystals. In *Semiconductor Nanocrystal Quantum Dots*; Rogach, A. L., Ed.; Springer: Vienna, 2008; pp 1−34.

(29) Guo, Q.; Kim, S. J.; Kar, M.; Shafarman, W. N.; Birkmire, R. W.; Stach, E. A.; Agrawal, R.; Hillhouse, H. W. *Nano Lett.* **2008**, *8*, 2982.

(30) Reiss, P. Synthesis of Semiconductor Nanocrystals in Organic Solvents. In *Semiconductor Nanocrystal Quantum Dots*; Rogach, A. L., Ed.; Springer: Vienna, 2008; pp 35−72.

(31) Yi, L.; Tang, A.; Niu, Mu.; Han, W.; Hou, Y.; Gao, M. *CrystEngComm* **2010**, *12*, 4124.

(32) Ahmadi, M.; Pramana, S. S.; Xi, L.; Boothroyd, C.; Lam, Y. M.; Mhaisalkar, S. *J. Phys. Chem. C* **2012**, *116*, 8202.

(33) Ng, M. T.; Boothroyd, C. B.; Vittal, J. J. *J. Am. Chem. Soc.* **2006**, *128*, 7118.

(34) Dai, P.; Shen, X.; Lin, Z.; Feng, Z.; Xu, H.; Zhan, J. *Chem. Commun.* **2010**, *46*, 5749.

(35) Pan, D.; An, L.; Sun, Z.; Hou, W.; Yang, Y.; Yang, Z.; Lu, Y. *J. Am. Chem. Soc.* **2008**, *130*, 5620.

(36) Wang, J.-J.; Wang, Y.-Q.; Cao, F.-F.; Guo, Y.-G.; Wan, L.-J. *J. Am. Chem. Soc.* **2010**, *132*, 12218.

(37) Shavel, A.; Arbiol, J.; Cabot, A. *J. Am. Chem. Soc.* **2010**, *132*, 4514.

(38) McBride, J. R.; Lupini, A. R.; Schreuder, M. A.; Smith, N. J.; Pennycook, S. J.; Rosenthal, S. J. *ACS Appl. Mater. Interfaces* **2009**, *1*, 2886.

(39) Marcano, G.; de Chalbaud, L. M.; Rincón, C.; Sánchez Pérez, G. *Mater. Lett.* **2002**, *53*, 151.

(40) Marcano, G.; Rincón, C.; López, S. A.; Sánchez Pérez, G.; Herrera-Pérez, J. L.; Mendoza-Alvarez, J. G.; Rodríguez, P. *Solid State Commun.* **2011**, *151*, 84.

(41) Kroumova, E.; Aroyo, M. I.; Perez-Mato, J. M.; Kirov, A.; Capillas, C.; Ivantchev, S.; Wondratschek, H. *Phase Transitions* **2003**, *76*, 155.

(42) Altosaar, M.; Raudoja, J.; Timmo, K.; Danilson, M.; Grossberg, M.; Krustok, J.; Mellikov, E. *Phys. Status Solidi A* **2008**, *205*, 167.

(43) Witte, W.; Kniese, R.; Powalla, M. *Thin Solid Films* **2008**, *517*, 867.

(44) Uday Bhaskar, P.; Suresh Babu, G.; Kishore Kumar, Y. B.; Sundara Raja, V. *Appl. Surf. Sci.* **2011**, *257*, 8529.

(45) Zhong, H.; Lo, S. S.; Mirkovic, T.; Li, Y.; Ding, Y.; Li, Y.; Scholes, G. D. *ACS Nano* **2010**, *4*, 5253.

(46) Li, Y. C.; Zhong, H. Z.; Li, R.; Zhou, Y.; Yang, C. H.; Li, Y. F. *Adv. Funct. Mater.* **2006**, *16*, 1705.

(47) Poznyak, S. K.; Osipovich, N. P.; Shavel, A.; Talapin, D. V.; Gao, M.; Eychmüller, A.; Gaponik, N. *J. Phys. Chem. B* **2005**, *109*, 1094.

(48) Wang, J.-J.; Hu, J.-S.; Guo, Y.-G.; Wan, L.-J. *NPG Asia Mater.* **2012**, *4*, e2.